water

MDPI

Article

Research on Descaling Characteristics and Simulation Calculation of a Coaxial High-Frequency Electronic Descaling Device

Yan Zhao [1], Lixin Zhang [1,*], Xin Zhao [2], Jin Liu [1] and Ming Gao [1]

[1] School of Energy and Power Engineering, University of Shanghai for Science and Technology, 516 Jungong Road, Shanghai 200093, China; usst_zhaoyan@126.com (Y.Z.); liujinusst@163.com (J.L.); gmvvv@163.com (M.G.)
[2] School of Computer Science, Central South University, 932 Lushan South Road, Changsha 410083, China; zhaoxin567@csu.edu.cn
* Correspondence: uzlx1@126.com

Abstract: High-frequency electronic descaling devices are physical water treatment methods that use a high-frequency electromagnetic field to prevent and remove scale. The effectiveness of the method is verified by monitoring the growth of scale on the surface of heat exchange tubes. The microstructure of scale obtained from experiments is analyzed by scanning electron microscope (SEM), and the action characteristics of high-frequency electromagnetic fields on water are explored by observing the change of solution contact angle at different times. The experimental results show that the high-frequency electromagnetic field can slow down the scaling growth on the surface of heat exchange tubes by changing the morphology of scaling substances and the physicochemical properties of water. The cavity of the instrument is modeled and simulated by ANSYS Maxwell, and the three operating parameters, waveform, voltage and frequency, are changed respectively. The performance parameters of the cavity, such as magnetic field energy, electric field energy and magnetic flux, are calculated and compared, and then the more suitable operating parameters are selected to improve the performance of the instrument. The simulation results show that the high-frequency electromagnetic field generated by the anode rod in the axial position can be overlooked compared with the magnetic field energy. Square wave excitation produces greater magnetic field energy than using sine wave excitation, and as the voltage increases, the peak value of the magnetic field energy continues to rise and increases faster. With an increase in the frequency, the peak value of the magnetic field energy and magnetic flux peak will maintain a slight decrease over a certain frequency range. After this frequency range, the peak value of magnetic field energy and magnetic flux peak will decrease rapidly. This decrease is due to the relaxation caused by the change of the waveform direction. The influence of time and an increase in the frequency will significantly increase the influence of the relaxation time.

Keywords: descaling; electromagnetic fields; electromagnetic induction; frequency; voltage; waves

check for updates

Citation: Zhao, Y.; Zhang, L.; Zhao, X.; Liu, J.; Gao, M. Research on Descaling Characteristics and Simulation Calculation of a Coaxial High-Frequency Electronic Descaling Device. *Water* **2021**, *13*, 789. https://doi.org/10.3390/w13060789

Academic Editor: Mika Sillanpää

Received: 15 February 2021
Accepted: 11 March 2021
Published: 14 March 2021

Publisher's Note: MDPI stays neutral with regard to jurisdictional claims in published maps and institutional affiliations.

Copyright: © 2021 by the authors. Licensee MDPI, Basel, Switzerland. This article is an open access article distributed under the terms and conditions of the Creative Commons Attribution (CC BY) license (https://creativecommons.org/licenses/by/4.0/).

1. Introduction

The circulating cooling water acts as the heat exchange medium in industrial systems and removes the system's waste heat to ensure the safe operation of the industrial system [1]. However, mineral ions, such as calcium and magnesium, in the circulating cooling water will be deposited on the metal heat exchange surface and pipeline to form fouling [2]. The composition of the fouling is complex, but the most common fouling is calcium carbonate [3,4]. The deposition rate of fouling will gradually accelerate with an increase in the concentration ratio of the circulating cooling water [5]. The thermal conductivity of fouling is very small, which will greatly weaken the heat transfer performance of the heat exchanger [6,7]. Because fouling growth is inevitable, the influence of fouling on

heat transfer resistance should be considered in the design of heat exchangers, as fouling increases the initial investment cost [8,9]. The growth of fouling in the pipeline increases the flow resistance, which, thus, increases the power consumption of the pump and affects the service life of the pipeline components [4,10]. These damages will increase the operating costs of industrial systems and create challenges in terms of the safe operation of industrial systems [5,11,12].

The common treatment method of circulating cooling water is to use chemical agents to curb the growth of the fouling layer. However, improving large amounts of a circulating water body and complex water quality environments often requires the use of multiple chemicals and large monetary investments, which increases the cost of water treatment and the risk of sewage discharge [8,13]. Physical water treatment methods based on magnetic, electric and electromagnetic fields have the advantages of environmental protection and energy savings, so they have received more attention and research [4,6,13–20].

Magnetic fields can change the physical and chemical properties of water, such as decreasing of surface tension and increasing of viscosity, which, in turn, affects the kinetic process of the chemical reactions [21–23]. However, the descaling effect of a magnetic field is affected by many factors. For example, the performance of the magnetic field is affected by the pipe wall material, and a better scale inhibition and descaling effect can be obtained when the magnetic field direction and fluid flow direction are orthogonal [24]. The pH value of the water has a great influence on the scale inhibition effect of the magnetic field. The growth of calcium carbonate crystals is inhibited by a magnetic field in a low-pH calcium carbonate solution but is only slightly affected by a magnetic field at high pH [25,26].

When the voltage signal is applied to the two parallel electrodes, the electric field generated between the electrodes can slow down the calcium carbonate scaling [6]. Xu et al. observed the changes in calcium carbonate crystals that were formed when the voltage amplitude was changed and found that the formed calcium carbonate crystals gradually changed from acicular aragonites to spherical aragonites with an increase in the voltage amplitude [6]. Tijing et al. explored the change in the fouling by changing the frequency of the voltage (10 V, 1.00 kHz–13.56 MHz) [27]. The experimental results showed that a decrease in the thermal resistance of the fouling gradually increased with an increase in the frequency, so high-frequency electric fields have a good descaling ability [19].

In addition to magnetic and electric fields, high-frequency electromagnetic fields also show excellent descaling ability. Common high-frequency electromagnetic field devices have either coaxial or solenoid structures. This kind of device is usually called electronic anti-fouling (EAF) technology [17,20,28]. Although other names have been used, its principle is based on Faraday's law of electromagnetic induction and should be different from other types of electronic water processors [20]. Cho et al. explained the EAF action mechanism and observed a decrease in the fouling resistance after installing solenoid winding on the inlet pipe of the heat exchanger. This work verified the effectiveness of EAF [28,29]. Zhang et al. studied the descaling characteristics of coaxial high-frequency electronic descaling devices and solenoid type induction electronic descaling devices, respectively [16,17]. The results showed that the hardness of the circulating cooling water decreased more greatly under the action of a high-frequency electronic descaling device, and the high-frequency electronic descaling device showed better scale inhibition characteristics. Induction-type electronic descaling devices have certain descaling characteristics, but their influence on the fouling growth is lower than that of the high-frequency electronic descaling devices.

The mechanism of scale inhibition and descaling by high-frequency electromagnetic fields is still controversial [20,30], but its effectiveness is undoubtedly confirmed and many scholars have observed changes in the crystal morphology and changes in the physical and chemical properties of aqueous solutions in experiments [15]. In a recent literature review, Lin et al. summarized many research papers and proposed that the Lorentz force is the main action mechanism [5,31]. At the same time, the transmission of electromagnetic

field energy to the circulating water system leads to an increase in the free energy of the system [32]. The energy of the electromagnetic field provides the necessary energy for crystal nucleation and improves the water activity, while the higher magnetic induction intensity inhibits the crystal growth.

This type of electronic descaling device can be manufactured through the design of electronic circuits and the installation of electrical components. The low use cost and lower environmental risk increase the competitiveness of electronic descaling devices in the field of industrial descaling technology. However, most of the research on this type of instrument has focused on the experimental verification of the descaling effectiveness, and there have been only a few reports on the relationship between the operating parameters and the performance of this type of instrument. The enhancement of the descaling ability of high-frequency electronic descaling devices is essentially the optimization of the technical electromagnetic field parameters, which are specifically reflected in the waveform, voltage, and frequency selection of the electromagnetic field generating device. The technical parameters of high-frequency electronic descaling devices determine the intensity and energy of the excited electromagnetic field. The development of related equipment has paid more attention to the optimization of related parameters, thereby increasing the electromagnetic field energy inside the cavity.

Research into the coaxial cavity structures is focused on the electrical field, mainly for UHV power transmission technology, high-temperature superconducting technology and other related electromagnetic research [33–35]. The different application background limits the cavity material and operating parameter settings. Differences in the research direction also lead to different analysis parameters and diversification of research methods.

In this paper, ANSYS Maxwell is used to model and simulate the cavity of a coaxial high-frequency electronic descaling device and to explore the influence of the operating parameters on the cavity performance. By changing the waveform, the field energy is compared and analyzed, and the best waveform is selected. By changing the voltage amplitude, the peak value of the magnetic field energy is compared, and the change in the magnetic field intensity along the axial direction of the cavity is analyzed. By changing the frequency, the peak and the decrease in the amplitude of the magnetic energy and the magnetic flux are analyzed, and a more appropriate frequency range is selected, which provides a reference for product design and the optimization of the related high-frequency electronic descaling devices. Through the self-designed fouling monitoring device, the growth of fouling is monitored online in real time, the morphology growth of the crystal is analyzed by SEM, and the contact angle is measured to analyze the characteristic changes of the water body. The simulation calculation of the high-frequency electromagnetic field helps to analyze the influence of operating parameters on electromagnetic field performance parameters. Through experimental research and simulation calculations, a more comprehensive analysis of the descaling characteristics of the high-frequency electromagnetic fields has been carried out.

2. Experimental Principle and Experimental System

2.1. Mechanism of a High-Frequency Electronic Descaling Device

The structure of a high-frequency electronic descaling device is shown in Figure 1 and is mainly composed of the high-frequency signal control unit, electrodes and pipe cavity. The electrodes connected to the control unit will generate induced charge with time, and the two electrodes, having equal but opposite charges, will generate an alternating electric field. According to Faraday's electromagnetic induction theory, an alternating electric field will induce alternating magnetic field, and both of these fields excite each other to produce an alternating electromagnetic field. An alternating electromagnetic field can change the physical and chemical properties of water, such as increasing the electrical conductivity, decreasing surface tension and increasing the solubility. The changes in these properties in turn achieve the goal of dissolving water scale, removing rust and sterilization. This

method is an ideal physical water treatment technology and does not require the use of chemical agents.

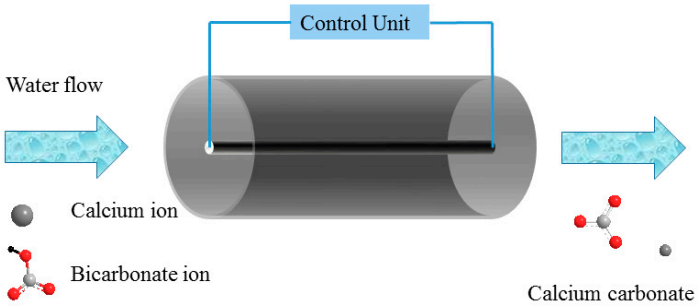

Figure 1. Mechanism of a high-frequency electronic descaling device.

2.2. Experimental System

As shown in Figure 2, the main equipment of the experimental system includes a cooling tower, pump, float flowmeter, heating unit, EAF, fouling monitoring device, data acquisition instrument, computer, etc. The water pump pumps out the water in the water tray of the cooling tower, which then flows through the heating unit to raise the temperature, enters the cooling tower after EAF treatment, and the circulating water is then uniformly sprayed on the filler and the fouling monitoring device and finally flows into the water tray of the cooling tower. The diameter of the cooling tower is 0.6 m, the height is 1.2 m, the flow rate of circulating water is 3 m^3/h and the heating unit uses three heating rods (single MAX 5 KW) in parallel to maintain the outlet temperature of the heating unit at 37 °C (±1.0 °C).

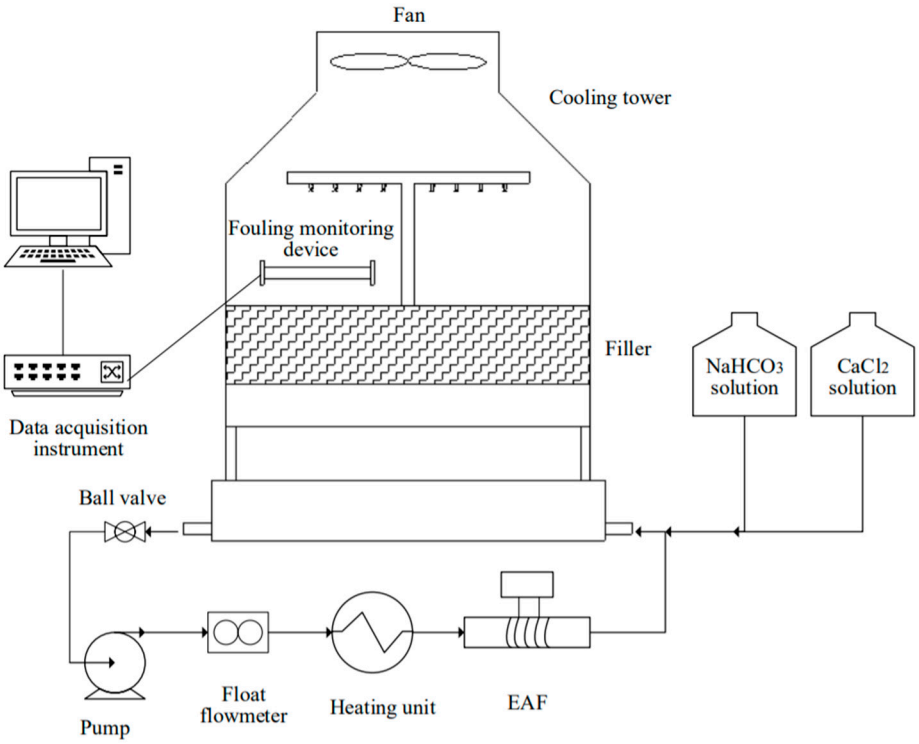

Figure 2. Experimental system diagram.

The fouling monitoring device is shown in Figure 3, which mainly consists of a stainless steel electric heating rod, brass pipe, fixing bracket, sealing end, etc. The stainless-steel electric heating rod has a diameter of 10 mm, a length of 300 mm and a maximum

heating power of 1 KW. The brass tube has a length of 360 mm, an inner diameter of 20 mm and a wall thickness of 4 mm. The stainless steel electric heating rod is fastened to the center of the brass tube through a fixed terminal, and the cavity is filled with magnesium oxide powder to make the heat conduction more uniform.

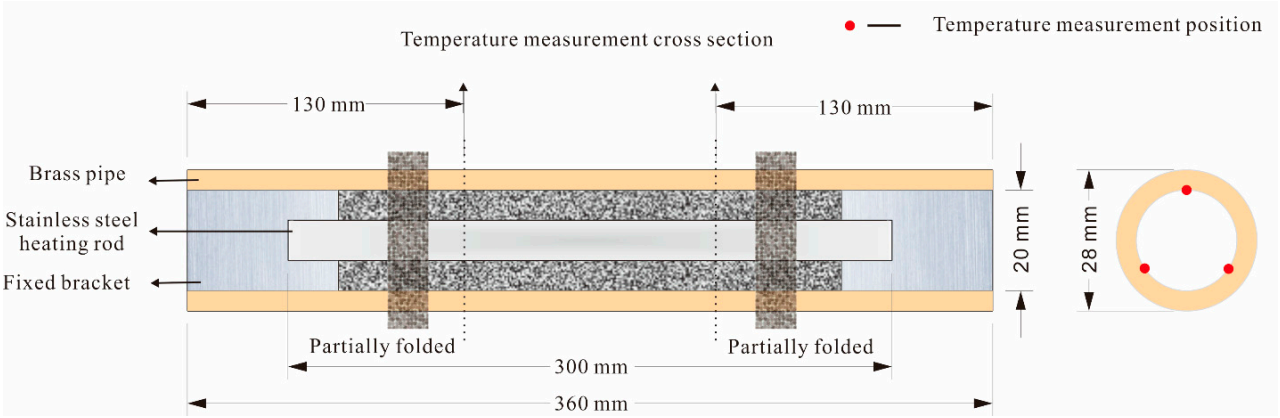

Figure 3. The fouling monitoring device.

In order to accelerate the scaling speed of the fouling monitoring device, the water hardness was improved by manual dosing. The total circulating water volume was 80 L, the initial water hardness was 80 mg/L (as $CaCO_3$), and the water hardness was adjusted to 1000 mg/L. The information and metering of added chemicals are shown in Table 1. The water replenishing increases the hardness to 1000 mg/L through the same artificial dosing method to maintain the same hardness as the initial water quality of the experiment, and the water quantity of water replenishing is adjusted by float valve.

Table 1. Detail of chemicals and dosage.

Items	Anhydrous Calcium Chloride	Sodium Bicarbonate
Purity (%)	≥97	≥99.5
Dosage (g)	66.6	100.8
Chemical formula	$CaCl_2$	$NaHCO_3$
Relative molecular mass	110.99	84.01

2.3. Experimental Principle

The calculation of fouling resistance can be calculated by the relevant heat transfer formula, and the symbols, names and units involved are explained as shown in Table 2. For the fouling monitoring device, according to the law of conservation of energy, after the experimental conditions are stable the heating amount Q_1 of the stainless steel electric heating tube is equal to the heat dissipation amount Q_2 of the brass tube in the system on both sides through the scale to spraying water, as shown in the following equation:

$$Q_1 = Q_2 = K_0 A \Delta t = K_2 A (T_b - T_s) \quad (1)$$

The temperature T_w of the inner wall of the brass tube is measured by a thermocouple, and the temperature T_b of the outer wall of the copper tube can be calculated by the following equation:

$$Q_1 = A \frac{T_w - T_b}{2\pi K_1 \frac{\ln D_2}{\ln D_1}} \quad (2)$$

Here, the spray water temperature T_s at the heat exchange copper pipe is used as the qualitative temperature of the water film. The fouling heat transfer coefficient K_1 can be calculated by the following equation:

$$K_2 = \frac{P}{A(T_b - T_0)} \tag{3}$$

The fouling resistance R_f is calculated by the following equation:

$$R_f = \frac{1}{K_2(t)} - \frac{1}{K_2(t=0)} \tag{4}$$

Table 2. Nomenclature of symbol, name, and unit.

Symbol	Characteristic	Unit
K_0	overall heat transfer	$Wm^{-2}\ K^{-1}$
K_1	Heat transfer coefficient of copper pipe	$Wm^{-2}\ K^{-1}$
K_2	Total heat transfer coefficient of scale layer	$Wm^{-2}\ K^{-1}$
A	Heat exchange area (outside surface)	m^2
T_w	Temperature of inner wall surface of brass pipe	K
T_b	Temperature of outer wall surface of brass pipe	K
T_s	Water film temperature of spray water	K
D_1	Inner diameter of brass pipe	m
D_2	Outer diameter of brass pipe	m
P	Heating power of heating rod in fouling monitoring device	W
R_f	fouling resistance	$m^2\ KW^{-1}$

3. Experimental Results and Discussion

3.1. Results and Discussion of Fouling Resistance

Temperature and power can be automatically recorded by the data acquisition instrument and transmitted to the computer, and a group of average values can be recorded every 10 s, with a running time of 18 h. In the experimental part, use EAF instead of high-frequency electronic descaling device description, which is mentioned in the introduction. The EAF operating conditions of the experimental group are square wave, 50 V, 10 MHz, and the inner wall temperature is 45.6 °C when the pipe wall is smooth. Figure 4 shows the relationship between the growth of fouling on the outer surface of the monitoring device at a temperature above 45 °C with or without EAF treatment over time.

It can be seen from Figure 4 that when EAF treatment is not carried out, the growth trend of fouling resistance changes, but the overall trend is upward. Without EAF, the scale experienced a process of increasing and decreasing in the first five hours, because the scale was peeled off by the shear force of spray water while growing rapidly, but the scale was still increasing. With the increase of running time, the effect of denudation gradually weakened and the scale entered a rapid growth period as long as 5 h, and then the growth rate slowed down but the scale continued to deposit.

It can be seen from Figure 4 that the fouling resistance with EAF treatment is significantly reduced, and the fouling resistance presents a wavy change form of slow increase and slow decrease in the running time as long as 18 h. At 18 h, the fouling resistance outside the pipe without EAF treatment is 5.00×10^{-5} (m^2 K)/W, and that outside the pipe with EAF treatment is 1.18×10^{-4} (m^2 K)/W, and the scale inhibition effect of EAF is remarkable during operation. Therefore, the operating parameters of EAF under this experimental condition are valid parameters, and subsequent modeling and simulation

calculations can be carried out according to this set of parameters, which is more conducive to improving the reliability of simulation results.

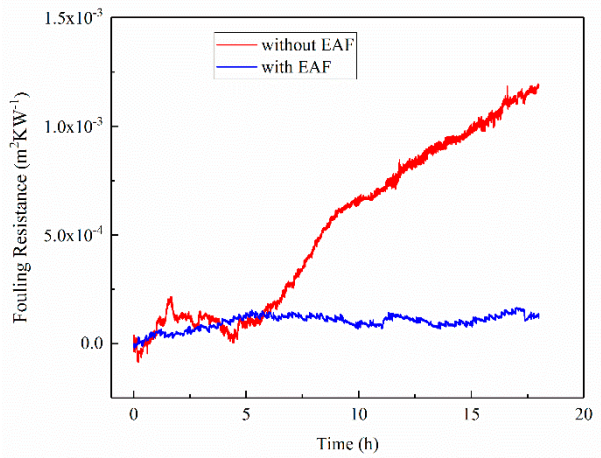

Figure 4. The trend of fouling resistance over time: with and without electronic anti-fouling (EAF) treatment at outer surface temperatures above 45 °C.

3.2. Results and Discussion of Microscopic Morphology of Scale Samples

In order to further explore the mechanism of EAF, the sample on the outer surface of the fouling monitoring device was collected by a scraper after the experiment, and then the sample was vacuum dried for SEM. Figure 5a shows the microscopic morphology of scale without EAF treatment. From this figure, it can be found that the appearance of particles is a hexahedron structure; each surface is flat, the ridge line is clear and the whole structure of scale formed by stacking a plurality of particles is dense. The sample on the outer surface of the cooling tower coil collected by Zhang et al. has the same hexahedral structure [16]. The sample on the inner surface of the water pipe collected by Sohaili et al. is mainly square and hexagonal calcite [10]. The morphology of these samples has the same characteristics as the morphology of the sample in this study (as shown in Figure 5a).

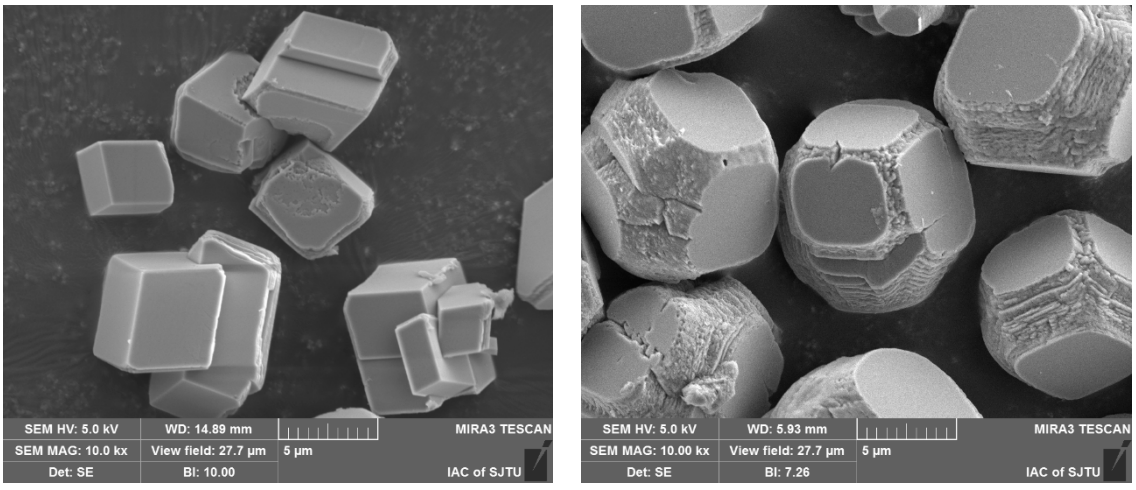

(**a**) Without EAF treatment (**b**) with EAF treatment

Figure 5. Microscopic morphology of scale samples.

Figure 5b shows the microscopic morphology of scale during EAF treatment. From the modification, it can be found that the ridge line of particles has subsided and the number of planes of the particles has increased. At this time, the overall structure of particles tends to be spherical, so the change of particle morphology makes it more difficult to stack

and grow. Figure 5a,b uses the same magnification throughout. It can be observed that the particle diameter of Figure 5b is obviously larger than that of Figure 5a. This result is consistent with the research conclusion of Zhang et al. [17], who reported the particle diameter increased from 4–8 μm (percentage 77%) to 6–11 μm (percentage 75%) after applying EAF; this was attributed to the promotion of electromagnetic fields. Therefore, EAF helps to accelerate the growth of fouling particles and condense them into spherical particles with larger volume, which makes the overall structure of fouling layers loose and easy to remove.

Xu et al. obtained sharp needle-shaped aragonite crystals (500 V) and spherical aragonite crystals (3000 V) using high-voltage electrostatic fields [6]. Zhang et al. used an induction-type electronic descaling device, and the collected aragonite had a needle-like structure and was densely stacked [16]. The crystal shape obtained in this study (as shown in Figure 5b) was spherical, and the structure was relatively loose. Different growth environments and descaling methods result in large differences in crystal structure.

3.3. Results and Discussion of Changes of Contact Angle

As shown in Figure 6, the contact angle of circulating water changes with time under the action of EAF. At a fixed time, 0.04 mL of circulating water sample was dropped on a brass plate through micro-dispenser, the brass plate having been polished and cleaned with 100 mesh sandpaper, and the contact angle was measured by software. It can be seen from Figure 6 that the decreasing speed of contact angle gradually decreased with the increase of time, but EAF could not continuously reduce the contact angle value of circulating water. The smaller the contact angle of circulating water, the stronger its wettability. Therefore, the circulating water can infiltrate into the scale layer, which is helpful for the scaling layer to fall off. The contact angle reflects the surface tension of liquid, and the surface tension of liquid with small contact angle will also decrease.

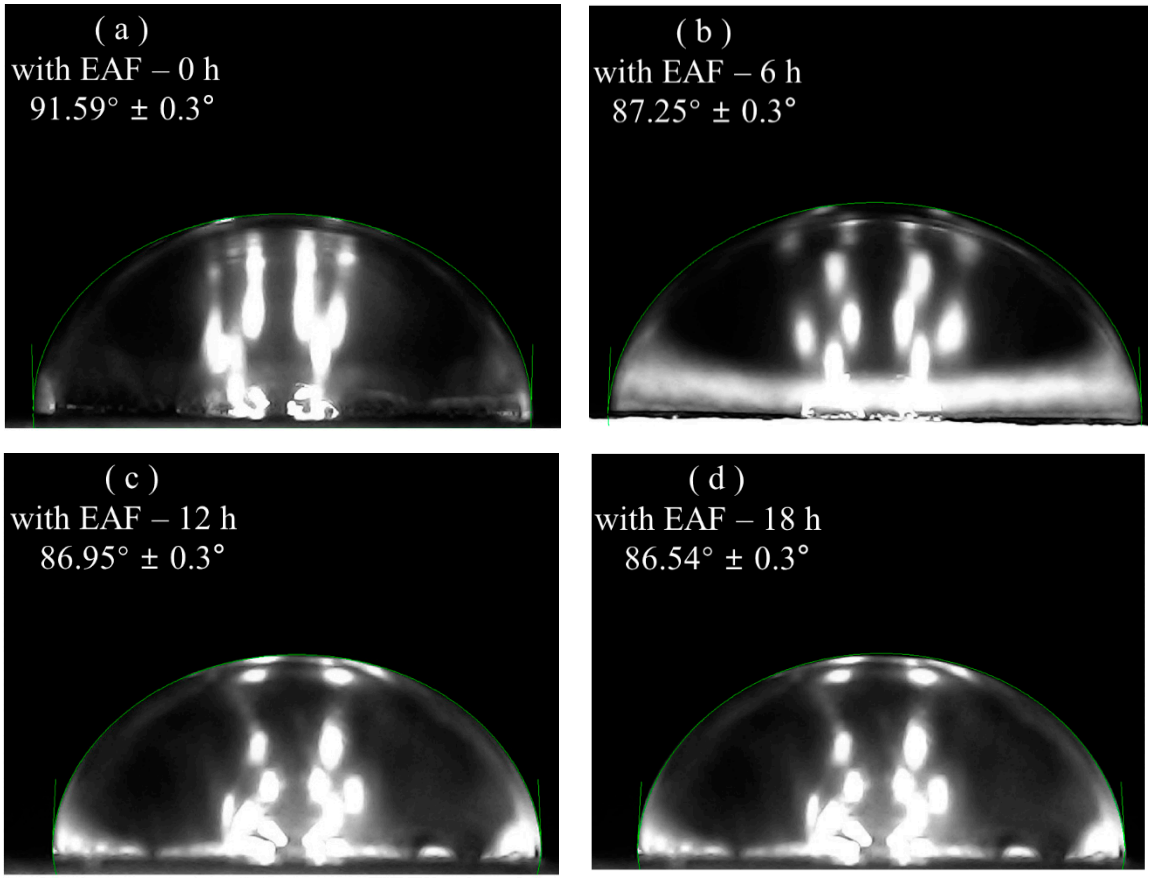

Figure 6. Changes of contact angles of circulating water with time under EAF.

This phenomenon shows that an electromagnetic field can effectively change the physical and chemical properties of water, which is because the distribution of molecules in water is changed by polarization. This phenomenon is similar to the phenomenon observed by Pang after using a magnetic field to act on water, which indicates that electromagnetic field has the effect of a magnetic field, so electromagnetic field scale removal technology has great research potential in the industrial field [22].

Otsuka et al. treated aeration pure water with a magnetic field for 2.5 h, and the contact angle of pure water on the copper plate was reduced by 10° [36]. Pang et al. also observed a decrease in the contact angle of pure water after applying a magnetic field [22]. The electromagnetic field acts on the water body, and the ions in the water are collided by the Lorentz force to combine and grow, so the number of colloidal particles in the water increases. Cho et al. found that an increase in the number of colloidal particles will increase the surface energy at the interface between water molecules and colloidal particles, and therefore the surface energy at the interface between water molecules and the wall will relatively decrease [37]. Lin et al. reported that the surface tension of water determines the interface interaction between water molecules and scale-forming ions or solid surfaces [5]. Based on the above research conclusions, the contact angle can be used as an index to evaluate an electromagnetic field's descaling ability.

Through the analysis of fouling resistance, microscopic morphology of scale samples and contact angles, the effectiveness of EAF technology was verified and its action characteristics were further analyzed. Under the action of an electromagnetic field, the morphology of fouling and the physical and chemical properties of water changed, and these changes were conducive to slow down the growth of scale.

The above experiments were carried out under a group of working conditions (square wave, 50 V, 10 MHz). The effect of EAF will be changed by changing the operating conditions, but a large number of experiments are needed to study. The modeling and simulation calculations of EAF will help to save workload and further study the variation characteristics of electromagnetic fields.

4. Model Simulation and Calculation

4.1. Cavity Physical Model

The high-frequency electronic descaling device is shown in Figure 7, and a 3D model of the electronic descaling cavity is established according to the real structure and is shown in Figure 8.

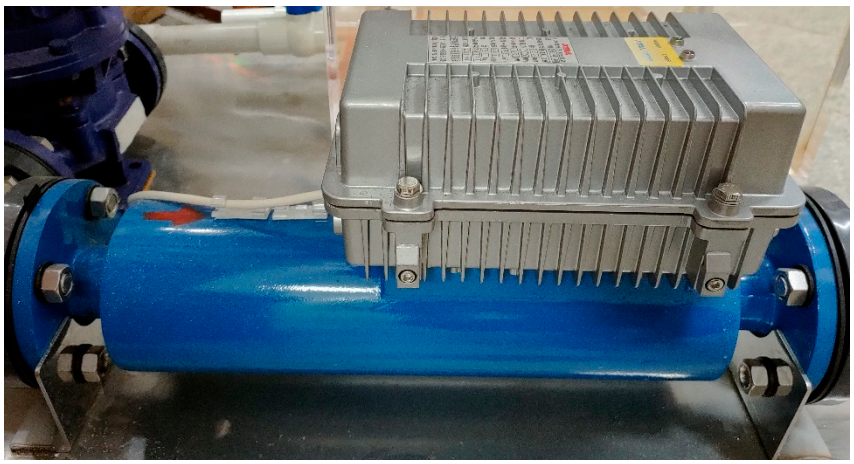

Figure 7. High-frequency electronic descaling device.

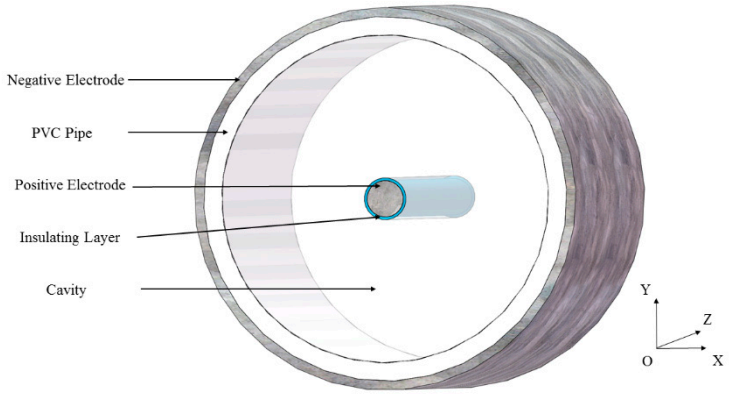

Figure 8. Cavity model.

The anode is a solid cylindrical stainless-steel rod with a diameter of 4 mm, and its length is 150 mm. The outer layer is wrapped with a 0.3 mm thick polytetrafluoroethylene material. The sleeve is a PVC plastic pipe with an outer diameter of 40 mm and an inner diameter of 36 mm. The cathode is made of stainless steel with a thickness of 1 mm wrapped outside the sleeve. The anode and cathode are not in direct contact with the liquid, to achieve a longer service life.

4.2. Calculation Conditions

According to the actual physical structure and size of the electronic descaling device used in the experiment, the three-dimensional space structure of the physical model is established and the parameters, such as the materials, are set. In this paper, the loaded excitation sources are time-varying analog signals, as shown in Figure 9, so the solution type is determined to be a transient field problem, and the solver is a 3D solver. Although the period corresponding to different frequencies varies, the time step is selected as one hundredth of the simulation period, and the simulation calculation ends after one period. The calculation unit is an eight-node hexahedron with a maximum error accuracy of 0.005. The area where the electromagnetic field changes drastically is finely divided, and then the meshing effect and quality of each part are verified, and the rough area is improved. The grid independence is verified. The electromagnetic field parameters, such as the magnetic field intensity and field energy of each point in the cavity, can be obtained by calculation.

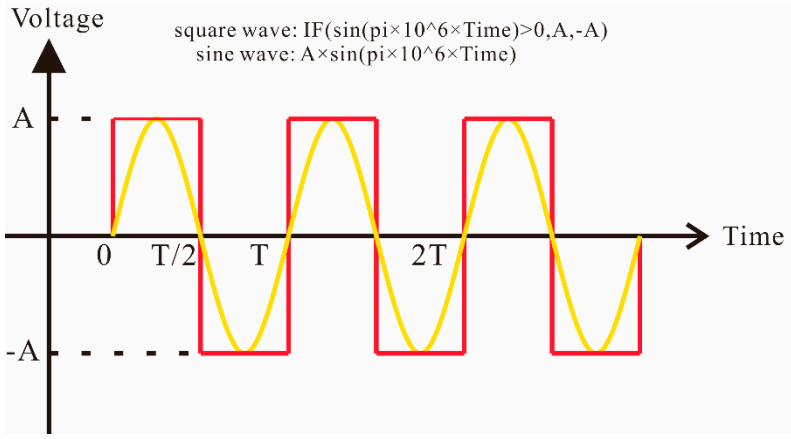

Figure 9. Loaded sine wave and square wave signal.

4.3. Electromagnetic Field Parameters

The parameters involved in the electromagnetic field analysis of the cavity include the electric field energy, magnetic field energy, magnetic field strength, magnetic flux, etc. What is obtained by the solver is only the electromagnetic field parameter value of the unit

grid. Therefore, to analyze the whole cavity in depth, post-processing calculations, such as summation, are required. The space volume of the unit grid is multiplied by the magnetic field energy density, and then the sum is accumulated to obtain the magnetic field energy ($Energy_M$) of the cavity at the transient time. Similarly, the electric field energy ($Energy_E$) of the cavity at the transient time can be obtained.

The magnetic field intensity (H) determines the force characteristics of the solution in the cavity. The goal of this research is to explore the magnetic field intensity characteristics of the cavity's axial plane (XOY plane). The magnetic field intensity is a vector, so lacks intuitive meaning. Because the structure of the cavity is fixed, the magnetic flux (Ø) is chosen as the comparison parameter. The magnetic flux can be obtained by multiplying the cavity's magnetic field intensity by the XOY plane.

5. Parameter Analysis

5.1. The Influence of Waveform Changes on the Electromagnetic Field

Given the same voltage amplitude (50 V) and frequency (0.5 MHz) settings, the electric field energy and magnetic field energy of the cavity under the action of a square and sine wave are calculated. Through data analysis, the change rules of the electric and magnetic field energies are the same, and the change in the magnetic field energy is shown in Figure 10.

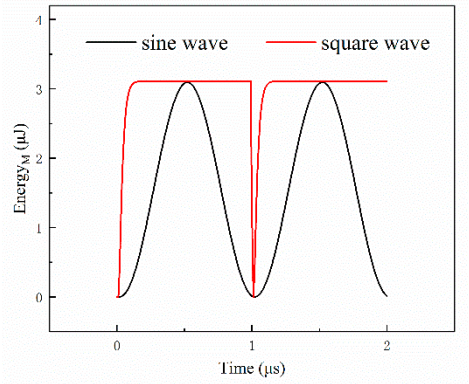

Figure 10. Comparison of cavity magnetic field energy when a sine wave and a square wave are applied (0.5 MHz, 50 V).

Figure 10 shows that the peak value of the magnetic field energy is approximately 0.003 J when excited by a sine wave or a square wave. However, when the square or sine wave is applied, the maximum electric field energy of the cavity is 6.45342×10^{-20} J or 1.39194×10^{-16} J, respectively. Therefore, no matter how the waveform changes, the electric field energy compared with the magnetic field energy can be ignored, and the influence of the frequency change can also be ignored. This shows that the high-frequency electronic descaling device used in this paper mainly affects the scaling process and transfers magnetic energy through the magnetic field. This finding is important for understanding the scaling mechanism of high-frequency electronic descaling devices.

Figure 10 shows that the magnetic field energy generated by the square wave is greater than that generated by the sine wave in the same cycle time. Therefore, when the square wave is applied, ions in the water can obtain more energy, which helps slow scaling on the wall. This is because the square wave changes in the direction of the voltage during a cycle, but the magnitude of the voltage does not change, so the energy generated by the square wave should be constant for any given time period in the cycle time. Because the sine wave changes over a period of time, the magnitude of the voltage is changing at all times, and the maximum value can be reached at one quarter and three quarters of the period. For the remainder of the time, the voltage value is less than the peak value. By summing the energy integrals over the entire cycle time, it is obvious from Figure 9 that the energy of the square wave is greater than that of the sine wave. At the same time, the impedance of the system is constant, and the current increases when the applied voltage increases.

According to the Biot–Savart law, the size of the current element determines the size of the magnetic induction. The square wave voltage is constant, so the current is constant and reaches a maximum value. The voltage of the sine wave can reach its maximum value at the peak value. Therefore, the square wave will generate more energy than the sine wave for the same amplitude and period. Therefore, when the square wave is applied, the ions in the water can obtain more energy, which helps to reduce the wall scaling.

The waveform change in the square wave in Figure 10 shows that when the direction of the square wave changes, the magnetic field energy of the cavity rapidly drops to zero and then returns to the peak value after a period of increase. In this paper, the time when the magnetic energy of the cavity increases from zero to the peak value due to the change in the wave direction is referred to as the relaxation time. During the relaxation time, the magnetic field energy is less than the peak value, which leads to a decrease in the magnetic field energy in the periodic time.

5.2. Influence of Voltage Amplitude Changes on Electromagnetic Field

Four groups of data with continuously changing voltage amplitudes (50 V, 100 V, 150 V, 200 V, and 250 V) are selected to calculate the magnetic field energy of the cavity in the case of a fixed square waveform and a frequency of 0.5 MHz. Figure 11 shows that, with an increase in the voltage amplitude, the peak value of the cavity magnetic field energy (MAX $Energy_M$) increases continuously. Although an increase in the voltage amplitude leads to an increase of relaxation time, the dominant factor influencing the sum of the cavity magnetic field energy in cycle time is the voltage amplitude at a fixed frequency.

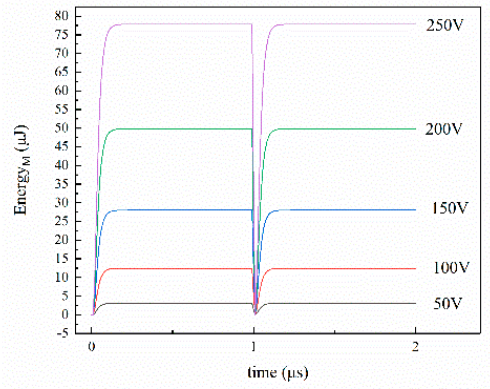

Figure 11. Variation in the cavity magnetic field energy with changes in the voltage.

As shown in Figure 12, the relationship between the voltage amplitudes from 50 V to 400 V and the peak value of the magnetic field energy is calculated. Figure 12 shows that the magnetic field energy increases with an increase in the voltage, and the growth rate of the magnetic field energy increases.

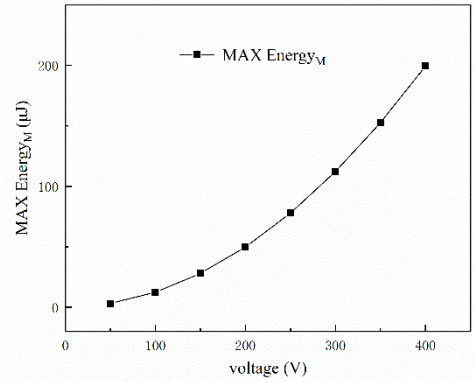

Figure 12. Variation of MAX $Energy_M$ with voltage value.

However, in the field, the voltage amplitude is limited to a certain extent because of safety restrictions. With an increase in the voltage, the energy of the cavity increases, but the actual scale inhibition ability does not increase with an increase in the voltage. On the one hand, an increase in the voltage can promote the collision of ions and accelerate the formation of crystals, but, at the same time, this increase will promote the crystal's decomposition into ions. There is a threshold voltage that the crystal growth rate reaches a maximum under the action of this voltage. Therefore, the voltage should be determined according to the actual water characteristics.

The model is an annular cavity, and the excitation source signals are uniformly applied on the inner and outer surfaces of the cavity. Therefore, the variation in the magnetic induction intensity along any radial direction from the origin in the XOY plane is the same. As shown in Figure 13, the magnetic induction intensity is distributed in concentric rings. The coordinate size of the cavity is shown in Figure 1. The component of the magnetic induction intensity along the Y-axis of the cavity s is calculated at a fixed frequency (0.5 MHz) and time (2×10^{-6} s) for different voltages, and the calculation results are shown in Figure 14.

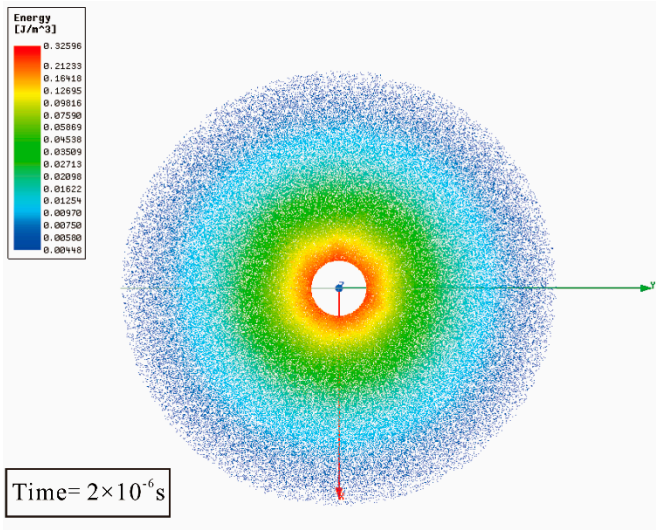

Figure 13. Magnetic field energy in the cavity (50 V, 0.5 MHz).

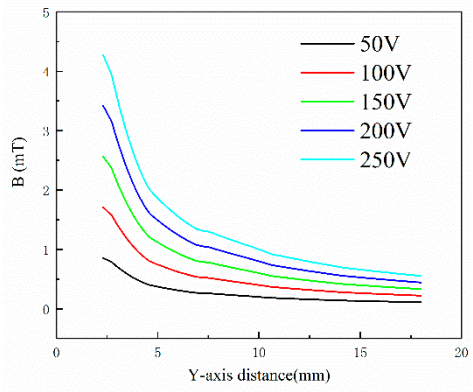

Figure 14. Changes in the magnetic flux density along the Y-axis of the cavity.

Figure 14 shows that the increase in the voltage amplitude will increase the magnetic induction intensity of the cavity's inner wall, and the magnetic induction intensity changes more sharply in the Y-axis direction. The magnetic induction intensity reaches its maximum value near the anode and decreases to its minimum value near the cathode (all values are greater than zero). The distribution of the magnetic induction intensity in the cavity is very uneven, and the electromagnetic field can play a certain role in scale inhibition for

a circulating cooling water system with a small circulating water volume. Currently, the research scale of the published reports is mostly focused on the laboratory scale and there are no actual field reports on the impact of a cooling water system with a large circulating water volume [6].

5.3. Influence of Frequency Changes on the Electromagnetic Field

With the fixed square wave waveform and 200 V parameter settings, 5 frequencies (0.5 MHz, 1 MHz, 5 MHz, 10 MHz, 20 MHz) are selected to calculate the magnetic field energy. Due to different periods, it is not possible to directly compare the magnetic field energy at a fixed time. The relaxation change value may be compared with the peak value, which may affect the evaluation. Therefore, the average and peak values of the magnetic field energy of the cavity within 2 μs are selected for comparison. The calculation results are shown in Table 3. It can be seen from Table 3 that with an increase in the frequency (0.5–10 MHz), the peak value of magnetic field energy in the cavity does not change much, but the average value of magnetic field energy decreases with an increase in the relaxation time proportion. When the frequency is 20 MHz, the decrease in the magnetic field energy is as much as 64%. Therefore, the applied voltage frequency does not result in an unlimited increase. Only when the frequency is controlled over a reasonable frequency range can the magnetic field energy of the cavity be maintained.

Table 3. The average and maximum value of the cavity magnetic field energy within 2 μs under variable frequency conditions.

Frequency (MHz)	Average (J)	MAX (J)	Decrease	Cycle Number
0.5	4.75704×10^{-5}	4.98124×10^{-5}	5%	1
1	4.61133×10^{-5}	4.98124×10^{-5}	7%	2
5	3.45778×10^{-5}	4.91981×10^{-5}	30%	10
10	2.25671×10^{-5}	4.45636×10^{-5}	49%	20
20	1.06845×10^{-5}	2.95166×10^{-5}	64%	40

To describe the variation of the cavity's magnetic induction intensity with frequency, the product of the magnetic induction intensity and the XOY surface, which is the magnetic flux, is selected to represent the intensity of the magnetic induction. The magnetic flux is scalar, so the numerical value can be compared directly. In the calculation, only the cavity is taken as a constraint to solve the problem. Therefore, the magnetic flux passing through the XOY surface is generated by the cavity. The average and maximum values of the magnetic flux passing through the XOY plane over 2 μs are shown in Table 4.

Table 4. The average and maximum value of cavity magnetic field energy within 2 μs under variable frequency conditions.

Frequency (MHz)	Average (Wb)	MAX (Wb)	Decrease	Cycle Number
0.5	9.73722×10^{-10}	1.00746×10^{-9}	3%	1
1	9.53964×10^{-10}	1.00746×10^{-9}	5%	2
5	7.94713×10^{-10}	1.00425×10^{-9}	21%	10
10	6.20447×10^{-10}	9.52905×10^{-10}	35%	20
20	4.11440×10^{-10}	7.75518×10^{-10}	47%	40

It can be seen from Table 4 that the maximum value of the magnetic flux in the frequency range of 0.5–5 MHz is relatively close and does not change significantly with frequency, and the influence of the relaxation time caused by the change in the square wave polarity is not obvious. However, the magnetic flux decreases with an increase in the magnetic flux. Because of the increasing peak drop amplitude caused by the relaxation time, the magnetic induction intensity gradually weakens. This is because there is loss on the stainless steel surface of the anode, and the resistance of the anode surface will continue

to increase as the frequency increases, resulting in an increase in the surface loss power of the boundary. When the increase caused by increasing the frequency cannot offset the power loss, the peak value of magnetic field energy and magnetic flux will decrease with an increasing frequency. This, of course, does not mean that a lower frequency is better. In the current study, a low-frequency (<2000 Hz) device did not observe significant descaling characteristics in a high-hardness circulating water scale inhibition experiment. The frequency cannot be increased continuously by synthesizing the two evaluation indexes: the magnetic field energy and magnetic flux. Maintaining the frequency in a reasonable range is helpful to enhance the magnetic field energy and magnetic induction intensity and strengthens the scale inhibition and descaling ability of the high-frequency electromagnetic field.

6. Conclusions

Through the experimental study of high-frequency electronic descaling instrument, it is observed that the growth of dirt is effectively inhibited by a high-frequency electromagnetic field, and the micro morphology of dirt and the physical and chemical characteristics of water are studied. The model and numerical calculations of the cavity are carried out. The magnetic field energy, electric field energy, magnetic induction intensity and magnetic flux are selected as the performance evaluation indexes. The effects of waveform, voltage and frequency on the electromagnetic field performance parameters are studied respectively.

(1) A high-frequency electromagnetic field is an effective physical descaling method. The formation of fouling on the heat transfer surface can be greatly reduced by a high-frequency electronic descaling device.
(2) Ahigh-frequency electromagnetic field accelerates the growth of scale particles and destroys their surface morphology, which makes the scale layer loose and easy to peel off.
(3) The contact angle decreases to a limited extent with the action of the high-frequency electromagnetic field, which is caused by the high-frequency electromagnetic field promoting the growth of water clusters and colloidal particles in the water. The contact angle can be used as an important index to measure the descaling ability of a high frequency electromagnetic field.
(4) For both square and sine waves, the electric field energy can be ignored compared with the magnetic field energy, so research on the mechanism of the high-frequency electromagnetic field produced by high-frequency electronic descaling devices should be focused on the role of the magnetic field.
(5) At the same amplitude and frequency, the magnetic field energy generated by the square wave is greater than that generated by the sine wave, so the high-frequency electronic descaling device with a square wave has better scale inhibition and descaling effects.
(6) Given the same frequency and square wave waveform, the energy of the magnetic field increases and the speed of growth is faster with an increase in the voltage. However, an excessively high voltage may lead to breaking molecular chains. The selection of the voltage amplitude needs to consider the promotion of crystallization and the role of molecular fracture.
(7) The descaling effect of the high-frequency electronic descaling device will not increase indefinitely as the frequency increases. Given a constant voltage and a square wave waveform, the peak values of the magnetic field energy and magnetic flux gradually decrease with an increase in the frequency. As the frequency increases, the influence of the relaxation time becomes more significant. Over a certain frequency range (0.5–5 MHz), changes in the magnetic field energy and magnetic flux are very small, so the design and selection of parameters can be carried out in this range.

Author Contributions: Conceptualization, Y.Z.; methodology, Y.Z.; software, X.Z.; validation, X.Z.; formal analysis, Y.Z.; investigation, J.L.; resources, L.Z.; data curation, L.Z.; writing—original draft

preparation, Y.Z.; writing—review and editing, X.Z.; visualization, X.Z.; supervision, J.L.; project administration, L.Z.; funding acquisition, M.G. All authors have read and agreed to the published version of the manuscript.

Funding: This research was funded by National Natural Science Foundation of China, grant number 51976127.

Institutional Review Board Statement: Not applicable.

Informed Consent Statement: Not applicable.

Data Availability Statement: All the data are represented in figures and tables. No other databases area.

Conflicts of Interest: The authors declare no conflict of interest.

References

1. Liu, B.C.; Cao, K.; Li, G.L.; Li, Y.Y.; Jia, W.G.; Zhang, Y.F. Experimental study on magnetic induction property of solenoid coil used in cooling water treatment system. *J. Water Supply Res Technol. Aqua* **2017**, *66*, 353–360. [CrossRef]
2. Teng, K.H.; Amiri, A.; Kazi, S.N.; Bakar, M.A.; Chew, B.T.; Al-Shamma'a, A.; Shaw, A. Retardation of heat exchanger surfaces mineral fouling by water-based diethylenetriamine pentaacetate-treated CNT nanofluids. *Appl. Therm. Eng.* **2017**, *110*, 495–503. [CrossRef]
3. Lee, G.J.; Tijing, L.D.; Pak, B.C.; Baek, B.J.; Cho, Y.I. Use of catalytic materials for the mitigation of mineral fouling. *Int. Commun. Heat Mass Transf.* **2006**, *33*, 14–23. [CrossRef]
4. Kim, W.; Cho, Y.I. Benefit of filtration in physical water treatment for the mitigation of mineral fouling in heat exchangers. *Int. Commun. Heat Mass Transf.* **2011**, *38*, 1008–1013. [CrossRef]
5. Lin, L.; Jiang, W.B.; Xu, X.S.; Xu, P. A critical review of the application of electromagnetic fields for scaling control in water systems: Mechanisms, characterization, and operation. *NPJ Clean Water* **2020**, *3*, 25. [CrossRef]
6. Xu, Z.M.; Chang, H.L.; Wang, B.B.; Wang, J.T.; Zhao, Q. Characteristics of calcium carbonate fouling on heat transfer surfaces under the action of electric fields. *J. Mech. Sci. Technol.* **2018**, *32*, 3445–3451. [CrossRef]
7. Kazi, S.N.; Teng, K.H.; Zakaria, M.S.; Sadeghinezhad, E.; Bakar, M.A. Study of mineral fouling mitigation on heat exchanger surface. *Desalination* **2015**, *367*, 248–254. [CrossRef]
8. Baig, H.; Antar, M.A.; Zubair, S.M. Performance evaluation of a once-through multi-stage flash distillation system: Impact of brine heater fouling. *Energy Conv. Manag.* **2011**, *52*, 1414–1425. [CrossRef]
9. Muller-Steinhagen, H.; Malayeri, M.R.; Watkinson, A.P. Heat Exchanger Fouling: Mitigation and Cleaning Strategies. *Heat Transf. Eng.* **2011**, *32*, 189–196. [CrossRef]
10. Sohaili, J.; Shi, H.S.; Lavania, B.; Zardari, N.H.; Ahmad, N.; Muniyandi, S.K. Removal of scale deposition on pipe walls by using magnetic field treatment and the effects of magnetic strength. *J. Clean Prod.* **2016**, *139*, 1393–1399. [CrossRef]
11. Kim, W.; Cho, D.J.; Cho, Y.I. Use of RF electric fields for simultaneous mineral and bio-fouling control in a heat exchanger. *Int. Commun. Heat Mass Transf.* **2011**, *38*, 1003–1007. [CrossRef]
12. Caputo, A.C.; Pelagagge, P.M.; Salini, P. Joint economic optimization of heat exchanger design and maintenance policy. *Appl. Therm. Eng.* **2011**, *31*, 1381–1392. [CrossRef]
13. Cho, Y.I.; Kim, W.T.; Cho, D.J. Electro-flocculation mechanism of physical water treatment for the mitigation of mineral fouling in heat exchangers. *Exp. Heat Transf.* **2007**, *20*, 323–335. [CrossRef]
14. Sronsri, C.; U-yen, K.; Sittipol, W. Quantitative analysis of calcium carbonate formation in magnetized water. *Mater. Chem. Phys.* **2020**, *245*, 122735. [CrossRef]
15. Raudino, M.; Sarri, F.; Tatini, D.; Ambrosi, M.; Aloisi, G.D.; Ninham, B.W.; Dei, L.; Lo Nostro, P. The Effect of Temperature and Magnetic Field on the Precipitation of Insoluble Salts of Alkaline Earth Metals. *J. Solut. Chem.* **2020**, *49*, 289–305. [CrossRef]
16. Zhang, L.X.; Li, X.; Gao, M.; Ma, L.; Zhao, S.X. Study on descaling characteristics of an induction-type electronic descaling device outside the heat transfer tubes of evaporative cooler. *Appl. Therm. Eng.* **2017**, *127*, 1627–1631. [CrossRef]
17. Zhang, L.X.; Chen, Y.B.; Gao, M.; Li, X.; Lin, Z.H. Validation of electronic anti-fouling technology in the spray water side of evaporative cooler. *Int. J. Heat Mass Transf.* **2016**, *93*, 624–628. [CrossRef]
18. Salman, M.A.; Al-Nuwaibit, G.; Safar, M.; Al-Mesri, A. Performance of physical treatment method and different commercial antiscalants to control scaling deposition in desalination plant. *Desalination* **2015**, *369*, 18–25. [CrossRef]
19. Tijing, L.D.; Lee, D.H.; Kim, D.W.; Cho, Y.I.; Kim, C.S. Effect of high-frequency electric fields on calcium carbonate scaling. *Desalination* **2011**, *279*, 47–53. [CrossRef]
20. Piyadasa, C.; Ridgway, H.F.; Yeager, T.R.; Stewart, M.B.; Pelekani, C.; Gray, S.R.; Orbell, J.D. The application of electromagnetic fields to the control of the scaling and biofouling of reverse osmosis membranes—A review. *Desalination* **2017**, *418*, 19–34. [CrossRef]
21. Cai, R.; Yang, H.W.; He, J.S.; Zhu, W.P. The effects of magnetic fields on water molecular hydrogen bonds. *J. Mol. Struct.* **2009**, *938*, 15–19. [CrossRef]

22. Pang, X.-F.; Deng, B.; Tang, B. Influences of magnetic field on macroscopic properties of water. *Mod. Phys. Lett. B* **2012**, *26*, 1250069. [CrossRef]
23. Chang, K.T.; Weng, C.I. The effect of an external magnetic field on the structure of liquid water using molecular dynamics simulation. *J. Appl. Phys.* **2006**, *100*, 043917. [CrossRef]
24. Alimi, F.; Tlili, M.M.; Ben Amor, M.; Maurin, G.; Gabrielli, C. Effect of magnetic water treatment on calcium carbonate precipitation: Influence of the pipe material. *Chem. Eng. Process.* **2009**, *48*, 1327–1332. [CrossRef]
25. Tai, C.Y.; Chang, M.C.; Shieh, R.J.; Chen, T.G. Magnetic effects on crystal growth rate of calcite in a constant-composition environment. *J. Cryst. Growth* **2008**, *310*, 3690–3697. [CrossRef]
26. Madsen, H.E.L. Crystallization of calcium carbonate in magnetic field in ordinary and heavy water. *J. Cryst. Growth* **2004**, *267*, 251–255. [CrossRef]
27. Tijing, L.D.; Kim, H.Y.; Lee, D.H.; Kim, C.S.; Cho, Y.I. Use of an oscillating electric field to mitigate mineral fouling in a heat exchanger. *Exp. Heat Transf.* **2009**, *22*, 257–270. [CrossRef]
28. Cho, Y.I.; Choi, B.G. Validation of an electronic anti-fouling technology in a single-tube heat exchanger. *Int. J. Heat Mass Transf.* **1999**, *42*, 1491–1499. [CrossRef]
29. Cho, Y.I.; Fan, C.; Choi, B.G. Theory of electronic anti-fouling technology to control precipitation fouling in heat exchangers. *Int. Commun. Heat Mass Transf.* **1997**, *24*, 757–770. [CrossRef]
30. Coey, J.M.D. Magnetic water treatment—How might it work? *Philos. Mag.* **2012**, *92*, 3857–3865. [CrossRef]
31. Koza, J.A.; Muhlenhoff, S.; Zabinski, P.; Nikrityuk, P.A.; Eckert, K.; Uhlemann, M.; Gebert, A.; Weier, T.; Schultz, L.; Odenbach, S. Hydrogen evolution under the influence of a magnetic field. *Electrochim. Acta* **2011**, *56*, 2665–2675. [CrossRef]
32. Zhao, J.D.; Liu, Z.A.; Zhao, E.J. Combined effect of constant high voltage electrostatic field and variable frequency pulsed electromagnetic field on the morphology of calcium carbonate scale in circulating cooling water systems. *Water Sci. Technol.* **2014**, *70*, 1074–1082. [CrossRef] [PubMed]
33. Nguyen, T.T.; Lee, W.G.; Lee, S.J.; Park, M.; Kim, H.M.; Won, D.; Yoo, J.; Yang, H.S. A simplified model of coaxial, multilayer high-temperature superconducting power cables with Cu formers for transient studies. *Energies* **2019**, *12*, 1514. [CrossRef]
34. Zhang, S.; Feng, H.S.; Zhuang, M.; Ding, K.Z.; Liu, C.L.; Zhou, Y.Q. Experimental research of a 10 kA HTS current lead using YBCO tapes. *IEEE Trans. Appl. Supercond.* **2020**, *30*, 1–7. [CrossRef]
35. Liang, J.H.; Chen, Z.H.; Wang, L.N. Magnetic field effect on critical current of different structural HTS DC cables. *IEEE Trans. Appl. Supercond.* **2019**, *29*, 1–3. [CrossRef]
36. Otsuka, I.; Ozeki, S. Does magnetic treatment of water change its properties? *J. Phys. Chem. B* **2006**, *110*, 1509–1512. [CrossRef] [PubMed]
37. Cho, Y.I.; Lee, S.H. Reduction in the surface tension of water due to physical water treatment for fouling control in heat exchangers. *Int. Commun. Heat Mass Transf.* **2005**, *32*, 1–9. [CrossRef]